Analytical and numerical modeling of an axisymmetrical electrostatic transducer with interior geometrical discontinuity

Petr Honzík,[a] Alexey Podkovskiy, Stéphane Durand, Nicolas Joly, and Michel Bruneau
LUNAM Université, LAUM (Laboratoire d'acoustique de l'université du Maine), UMR CNRS 6613, Avenue Olivier Messiaen, F-72085 Le Mans, France

(Received 18 January 2013; revised 20 June 2013; accepted 23 September 2013)

The main purpose of the paper is to contribute at presenting an analytical and a numerical modeling which would be relevant for interpreting the couplings between a circular membrane, a peripheral cavity having the same external radius as the membrane, and a thin air gap (with a geometrical discontinuity between them), and then to characterize small scale electrostatic receivers and to propose procedures that could be suitable for fitting adjustable parameters to achieve optimal behavior in terms of sensitivity and bandwidth expected. Therefore, comparison between these theoretical methods and characterization of several shapes is dealt with, which show that the models would be appropriate to address the design of such transducers. © *2013 Acoustical Society of America*. [http://dx.doi.org/10.1121/1.4824342]

PACS number(s): 43.38.Bs [MS] Pages: 3573–3579

I. INTRODUCTION

The two-dimensional axisymmetrical problem addressed here governs the behavior of acoustic fields in both an air gap and a peripheral cavity whose shapes are cylinders, coupled through an interior geometrical discontinuity between them (Fig. 1), and excited by the displacement field of a membrane, the outer dimension of the membrane being equal to the external dimension of the peripheral cavity. This specific transducer, herein a small scale electrostatic receiver, is assumed to be driven by a uniform time-periodic incident field. The main purpose of the paper is to characterize this device and to propose a procedure that could be suitable for fitting adjustable parameters to achieve optimal behavior of the receiver in terms of sensitivity and bandwidth expected.

The acoustic electrostatic receiver considered in this paper is, to some extent, inspired by an analogous device analyzed previously.[1–4] The two devices differ in only one respect. In the device analyzed previously, the peripheral cavity is set outside the periphery of the membrane such as the external dimension of the device is the dimension of the external periphery of this outer cavity. In the device considered herein, the peripheral cavity is set behind the peripheral part of the membrane such as the external dimension of the device is the dimension of the membrane, improving even the compactness of the device.

Then the work deals primarily with analytical methods which are appropriate to address this requirement, thermoviscous boundary layer effects and coupling effects are actually taken into account. The analytical method relies on eigenmodes expansions of both the membrane and the fluid-filled elements loading the membrane (air gap and peripheral cavities), along with general solutions of the associated homogeneous propagation equations (see, for example, Refs. 1, 4–8). The analytical approach used to provide the results given in this paper has been validated previously from comparison with experimental results obtained on similar transducers available in the literature.[5,7]

Regarding the numerical method which could be given also for final designs of devices, numerical simulation using an adaptive mesh and accounting for the viscous and thermal boundary layer effects[9–11] has been handled herein; particularly here, it provides more results against which the approximate analytical results can be tested.

Being concerned by the use of these models for the design of such transducers which involve compactness and flexibility (especially in terms of bandwidth), and actually by the characterization of this kind of device, several shapes, yet typical of applications, are considered below, and analytical and numerical results are compared together. These comparisons show that the methods suggested herein could provide information on geometrical parameters characterizing the air gap and the peripheral cavity on the working frequency range (related or not to resonance condition), and on the characteristics of the membrane to achieve the expected optimal performances.

Finally, the advantage of such a transducer design over the more classical one,[1] in terms of sensitivity and bandwidth, is presented.

II. ANALYTICAL SOLUTION

The two-dimensional axisymmetrical problem addressed here governs the behavior of acoustic pressure fields in small domains, namely, a fluid gap of thickness h_g in the interval $(0, R_e)$ and a peripheral cavity of thickness h_c in the interval (R_e, R_M), assumed to be excited by a membrane (acting as an extended time-periodic source) set at $z = 0$, R_e and R_M are the radii of the electrode and the membrane, respectively.

[a]Author to whom correspondence should be addressed. Electronic mail: petr.honzik@gmail.com

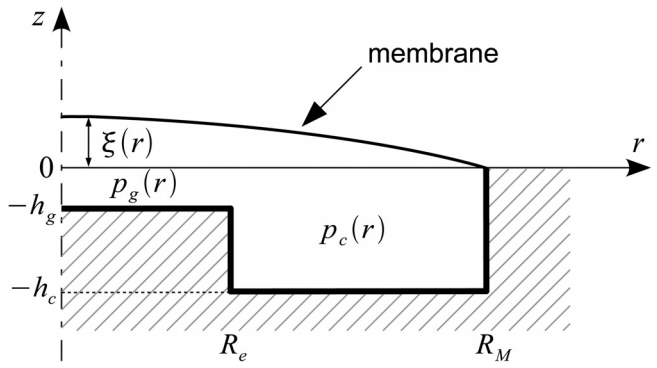

FIG. 1. Two-dimensional axisymmetrical half geometry of the transducer.

A. Equations governing the membrane displacement

The equation governing the vibration of the membrane driven by a harmonic incident acoustic pressure field p_{inc} (uniform over the membrane surface) and loaded by the pressure field $p(r)$ [namely, the pressure in the air gap, $p_g(r)$, and the cavity, $p_c(r)$], can be written as follows (given that the time dependence is $e^{j\omega t}$):

$$T(\Delta_r + K^2)\xi(r) = p_{inc} - p(r), \tag{1}$$

with

$$p(r) = \begin{cases} p_g(r), & r \in (0, R_e) \\ p_c(r), & r \in (R_e, R_M), \end{cases}$$

where $K^2 = \omega^2 m_S/T$ is the wavenumber of the free flexural vibration of the membrane, T is the tension of the membrane, $m_S = h_M \rho_M$ is the membrane mass per unit area (h_M and ρ_M are the membrane thickness and its density, respectively), and ω is the angular frequency. The membrane is clamped at its periphery $r = R_M$ [Dirichlet boundary condition $\xi(R_M) = 0$].

The general solution for the membrane displacement is the eigenfunction expansion

$$\xi(r) = \sum_n \xi_n \Psi_n(r) \tag{2}$$

with

$$\Psi_n(r) = \frac{1}{\sqrt{\pi} R_M J_1(K_n R_M)} J_0(K_n r), \tag{3}$$

where $J_\nu(x)$ is the νth order Bessel function of the first kind, K_n is given by the equation $J_0(K_n R_M) = 0$. Using the orthogonality properties of the eigenfunctions $\Psi_n(r)$, the constants ξ_n can be expressed as

$$\xi_n = \frac{1}{T(K^2 - K_n^2)} \iint_{S_M} (p_{inc} - p(r))\Psi_n \, dS_M, \tag{4}$$

where $S_M = \pi R_M^2$ is the surface of the membrane.

B. Equations governing the pressure variations

1. Behavior of fluid gap (slit) and flat annular cavity

Assuming usual approximations, namely, small harmonic acoustic perturbations, quasi-plane wave approximation, axial component of the particle velocity negligible against its radial component and derivatives with respect to radial coordinate of both particle velocity and temperature variation negligible against their derivatives with respect to axial coordinate, the solutions of the linearized version of the Navier–Stokes equation and the Fourier equation for heat conduction give, under several approximations, the particle velocity, v, and temperature variation, τ, profiles across the element (see Refs. 1, 12, and 13 for details). Introducing the mean values of these profiles (the subscripts v and h are related to the viscous and thermal effects, respectively, and the subscripts g and c are related to the fluid gap and cavity, respectively)

$$\bar{v}_{g,c}(r) = -\frac{1}{j\omega\rho_0} \partial_r p_{g,c}(r) F_{v(g,c)},$$
$$\bar{\tau}_{g,c}(r) = \frac{\gamma - 1}{\gamma \hat{\beta}} p_{g,c}(r) F_{h(g,c)}, \tag{5}$$

with

$$F_{(h,v)(g,c)} = 1 - \frac{\tan(k_{h,v} h_{g,c}/2)}{k_{h,v} h_{g,c}/2},$$
$$k_v = \frac{1-j}{\sqrt{2}} \sqrt{\rho_0 \omega/\mu}, \quad k_h = \frac{1-j}{\sqrt{2}} \sqrt{\rho_0 \omega C_P/\lambda_h}, \tag{6}$$

into the conservation of mass equation (accounting for the state equation) leads to the wave equation for the acoustic pressure in the backing acoustic elements

$$\Delta_r p_{g,c}(r) + \chi_{g,c}^2 p_{g,c}(r) = \zeta_{g,c} \xi(r), \tag{7}$$

the complex wavenumber and the source term are given, respectively, by

$$\chi_{g,c} = k_0 \sqrt{\frac{\gamma - (\gamma - 1) F_{h(g,c)}}{F_{v(g,c)}}} \tag{8}$$

($k_0 = \omega/c_0$ is the adiabatic wavenumber) and $\zeta_{g,c}\xi(r)$ with $\zeta_{g,c} = -\rho_0 \omega^2/(h_{g,c} F_{v(g,c)})$. The parameters which specify the nature of the fluid being the density ρ_0, the adiabatic speed of sound c_0, the ratio of specific heats γ, the shear dynamic viscosity μ, the thermal conductivity λ_h, the specific heat coefficient at constant pressure per unit of mass C_P, and the increase in pressure per unit increase in temperature at constant density $\hat{\beta} = (\partial P/\partial T)_\rho \cong P_0/T_0$ (P_0 and T_0 are the static pressure and the static temperature, respectively).

The analytical procedure used to describe the pressure field in the peripheral cavity (the variable of interest here) is a compromise between the numerical solution of the basic equations (namely, the Navier–Stokes equation and the

energy Fourier equation) subjected to the appropriate boundary conditions (see Sec. III) and the "small cavity" approximation which assumes that the acoustic pressure is uniform inside the peripheral cavity. This analytical procedure assumes that the pressure variation depends only on the r-coordinate all over the surface of the peripheral part of the membrane (this is valid almost everywhere as verified numerically; see Fig. 3) even though the domain is not very thin, avoiding intricate mathematics.

2. Acoustic pressure inside the transducer

The solution of the wave equation (7) for the acoustic pressure in the air gap is expressed as the sum of the general solution (of finite extent at $r = 0$) and the particular solution which takes the form of an expansion on the same eigenfunctions as for the membrane displacement

$$p_g(r) = A_g J_0(\chi_g r) + \sum_l p_{gl}\Psi_l(r), \text{ with } p_{gl} = \frac{\zeta_g \xi_l}{\chi_g^2 - K_l^2}. \quad (9)$$

When the radius of the peripheral cavity become much greater than its height, the radial component of the particle velocity predominates and the cavity acts as an annular slit. Then, the acoustic pressure in this cavity is given by [Eq. (7)]

$$p_c(r) = A_c J_0(\chi_c r) + B_c Y_0(\chi_c r) + \sum_l p_{cl}\Psi_l(r), \quad \text{with } p_{cl} = \frac{\zeta_c \xi_l}{\chi_c^2 - K_l^2}, \quad (10)$$

where $Y_\nu(x)$ is the νth order Bessel function of the second kind. The integration constant, B_c [Eq. (10)], is given by the vanishing radial particle velocity condition on the solid boundary at $r = R_M$ which leads to the Neumann boundary condition for the acoustic pressure in the cavity $\partial_r p_c(R_M) = 0$,

$$B_c = \frac{-\chi_c A_c J_1(\chi_c R_M) - \sum_l p_{cl}\frac{K_l}{\sqrt{\pi}R_M}}{\chi_c Y_1(\chi_c R_M)}. \quad (11)$$

The integration constants, A_g [Eq. (9)] and A_c [Eq. (10)], are given by the continuity conditions at the periphery of the fluid gap, $r = R_e$

(i) Continuity of the acoustic pressure, $p_g(R_e) = p_c(R_e)$.

(ii) Continuity of the acoustic volume velocity which leads to $F_{vg} h_g \partial_r p_g(R_e) = F_{vc} h_c \partial_r p_c(R_e)$.

The integration constants can then be expressed as

$$A_g = -\frac{1}{\mathcal{D}}\left(\mathcal{E}\sum_l \xi_l \mathcal{H}_l + \mathcal{F}\sum_l \xi_l \mathcal{J}_l\right),$$
$$A_c = \frac{1}{\mathcal{D}}\left(\mathcal{G}\sum_l \xi_l \mathcal{H}_l - J_0(\chi_g R_e)\sum_l \xi_l \mathcal{J}_l\right), \quad (12)$$

where

$$\mathcal{D} = \mathcal{E} J_0(\chi_g R_e) + \mathcal{F}\mathcal{G},$$
$$\mathcal{E} = F_{vc} h_c \chi_c \left(\frac{Y_1(\chi_c R_e) J_1(\chi_c R_M)}{Y_1(\chi_c R_M)} - J_1(\chi_c R_e)\right),$$
$$\mathcal{F} = J_0(\chi_c R_e) - \frac{Y_0(\chi_c R_e) J_1(\chi_c R_M)}{Y_1(\chi_c R_M)},$$
$$\mathcal{G} = F_{vg} h_g \chi_g J_1(\chi_g R_e),$$
$$\mathcal{H}_l = \frac{J_0(K_l R_e)}{\sqrt{\pi}R_M J_1(K_l R_M)}\left(\frac{\zeta_g}{\chi_g^2 - K_l^2} - \frac{\zeta_c}{\chi_c^2 - K_l^2}\right) + \frac{Y_0(\chi_c R_e)}{\chi_c Y_1(\chi_c R_M)}\frac{\zeta_c K_l}{\sqrt{\pi}R_M(\chi_c^2 - K_l^2)},$$
$$\mathcal{J}_l = \frac{K_l J_1(K_l R_e)}{\sqrt{\pi}R_M J_1(K_l R_M)}\left(\frac{F_{vg} h_g \zeta_g}{\chi_g^2 - K_l^2} - \frac{F_{vc} h_c \zeta_c}{\chi_c^2 - K_l^2}\right) + \frac{Y_1(\chi_c R_e)}{Y_1(\chi_c R_M)}\frac{\zeta_c K_l F_{vc} h_c}{\sqrt{\pi}R_M(\chi_c^2 - K_l^2)}. \quad (13)$$

C. Coupling between the membrane displacement and the acoustic pressure inside the transducer

Introducing both the acoustic pressure p_g and p_c in Eq. (4) gives

$$T(K^2 - K_n^2)\xi_n = p_{inc}\iint_{S_M}\Psi_n(r)\,\mathrm{d}S_M - \iint_{S_e} p_g(r)\Psi_n(r)\,\mathrm{d}S_e - \iint_{S_{eM}} p_c(r)\Psi_n(r)\,\mathrm{d}S_{eM}, \quad (14)$$

where $S_e = \pi R_e^2$ and $S_{eM} = \pi(R_M^2 - R_e^2)$, and leads after integration, to the following expression for the coefficients, ξ_n:

$$T(K^2 - K_n^2)\xi_n = b_n + \sum_l \xi_l C_{nl}, \quad (15)$$

or, in the matrix form

$$\{[\mathbb{U}] - [\mathbb{C}]\}(\Xi) = (B), \quad (16)$$

where (Ξ) and (B) are the column vectors of elements ξ_n and

$$b_n = \frac{2\sqrt{\pi}p_{inc}}{K_n}, \quad (17)$$

respectively, $[\mathbb{U}]$ is the diagonal matrix of elements $T(K^2 - K_n^2)$, and where the matrix $[\mathbb{C}]$ of elements C_{nl} is given by [after using Eqs. (9), (10), and (14)]

$$C_{nl} = \frac{\mathcal{R}_n}{\mathcal{D}}(\mathcal{E}\mathcal{H}_l + \mathcal{F}\mathcal{J}_l) - \frac{\mathcal{L}_n}{\mathcal{D}}(\mathcal{G}\mathcal{H}_l - J_0(\chi_g R_e)\mathcal{J}_l) - \mathcal{O}_{nl} - \mathcal{X}_{nl}, \quad (18)$$

with

$$\mathcal{L}_n = \frac{2\sqrt{\pi}}{R_M J_1(K_n R_M)}\left(\mathcal{M}_n - \frac{J_1(\chi_c R_M)}{Y_1(\chi_c R_M)}\mathcal{N}_n\right),$$

$$\mathcal{M}_n = \frac{R_e}{\chi_c^2 - K_n^2}\left[K_n J_0(\chi_c R_e)J_1(K_n R_e) - \chi_c J_1(\chi_c R_e)J_0(K_n R_e)\right] - \frac{R_M}{\chi_c^2 - K_n^2}K_n J_0(\chi_c R_M)J_1(K_n R_M),$$

$$\mathcal{N}_n = \frac{R_e}{\chi_c^2 - K_n^2}\left[K_n Y_0(\chi_c R_e)J_1(K_n R_e) - \chi_c Y_1(\chi_c R_e)J_0(K_n R_e)\right] - \frac{R_M}{\chi_c^2 - K_n^2}K_n Y_0(\chi_c R_M)J_1(K_n R_M),$$

$$\mathcal{O}_{nl} = \frac{2\zeta_c}{(\chi_c^2 - K_l^2)R_M^2 J_1(K_n R_M)}\left(\frac{\mathcal{Q}_{nl}}{J_1(K_l R_M)} - \frac{K_l \mathcal{N}_n}{\chi_c Y_1(\chi_c R_M)}\right),$$

$$\mathcal{Q}_{nl} = \begin{cases} \dfrac{R_M^2}{2}J_1^2(K_l R_M) - \dfrac{R_e^2}{2}\left[(J_0^2(K_l R_e) + J_1^2(K_l R_e)\right] & \text{for } l = n, \\ \dfrac{R_e}{K_l^2 - K_n^2}\left[K_n J_0(K_l R_e)J_1(K_n R_e) - K_l J_1(K_l R_e)J_0(K_n R_e)\right] & \text{for } l \neq n, \end{cases}$$

$$\mathcal{R}_n = \frac{2\sqrt{\pi}}{R_M J_1(K_n R_M)}\frac{R_e}{(\chi_g^2 - K_n^2)}\left[\chi_g J_1(\chi_g R_e)J_0(K_n R_e) - K_n J_0(\chi_g R_e)J_1(K_n R_e)\right],$$

$$\mathcal{X}_{nl} = \begin{cases} \dfrac{\zeta_g R_e^2}{R_M^2}\dfrac{J_0^2(K_l R_e) + J_1^2(K_l R_e)}{J_1^2(K_l R_M)(\chi_g^2 - K_l^2)} & \text{for } l = n, \\ \dfrac{2\zeta_g R_e}{R_M^2}\dfrac{K_l J_1(K_l R_e)J_0(K_n R_e) - K_n J_0(K_l R_e)J_1(K_n R_e)}{J_1(K_n R_M)J_1(K_l R_M)(\chi_g^2 - K_l^2)(K_l^2 - K_n^2)} & \text{for } l \neq n. \end{cases} \tag{19}$$

D. Pressure sensitivity

Once the amplitudes ξ_n of the membrane modes are calculated using Eq. (16), the mean displacement of the membrane over the surface of the electrode takes the form

$$\bar{\xi}_{S_e} = \frac{1}{S_e}\int\!\!\int_{S_e}\xi(r)\,\mathrm{d}S_e = \frac{2}{\sqrt{\pi}R_e R_M}\sum_n \xi_n \frac{J_1(K_n R_e)}{K_n J_1(K_n R_M)}. \tag{20}$$

The pressure sensitivity for the given polarization voltage, U_0, is then

$$\sigma = \frac{u}{p_{inc}} = -U_0\frac{\bar{\xi}_{S_e}}{p_{inc}h_g}. \tag{21}$$

III. NUMERICAL SOLUTION

The linearized versions (but, here, without any other approximations contrary to Sec. II B 1) of the Navier–Stokes equation, the conservation of mass equation, and the Fourier equation for heat conduction (accounting for the state equation) can be combined into the set of basic linear coupled equations for the particle velocity v and temperature variation τ.[9] The numerical modeling is based on this linear formulation discretized using Galerkin finite elements, the same mesh interpolation being used for particle velocity and temperature variation.[10] The corresponding weak form on the two-dimensional axisymmetrical fluid domain, Ω, takes the form (given that the time dependence is $\mathrm{e}^{j\omega t}$)

$$\begin{aligned}
&\int\!\!\int_\Omega \Big\{\omega^2\rho_0 v_r w_{vr} - j\omega\hat{\beta}\partial_r\tau w_{vr} \\
&\quad - \partial_r w_{vr}\Big[\left(\rho_0 c_0^2/\gamma + j\omega(4\mu/3+\eta)\right)\partial_r v_r \\
&\quad + \left(\rho_0 c_0^2/\gamma + j\omega(\eta - 2\mu/3)\right)(v_r/r + \partial_z v_z)\Big] \\
&\quad - w_{vr}\Big[\left(\rho_0 c_0^2/\gamma + j\omega(4\mu/3+\eta)\right)v_r/r \\
&\quad + \left(\rho_0 c_0^2/\gamma + j\omega(\eta - 2\mu/3)\right)(\partial_r v_r + \partial_z v_z)\Big]\Big/r \\
&\quad - j\omega\mu\partial_z w_{vr}(\partial_z v_r + \partial_r v_z)\Big\}\,\mathrm{d}\Omega = 0, \\
&\int\!\!\int_\Omega \Big\{\omega^2\rho_0 v_z w_{vz} - j\omega\hat{\beta}\partial_z\tau w_{vz} \\
&\quad - \partial_z w_{vz}\Big[\left(\rho_0 c_0^2/\gamma + j\omega(4\mu/3+\eta)\right)\partial_z v_z \\
&\quad + \left(\rho_0 c_0^2/\gamma + j\omega(\eta - 2\mu/3)\right)(v_r/r + \partial_r v_r)\Big] \\
&\quad - j\omega\mu\partial_r w_{vz}(\partial_z v_r + \partial_r v_z)\Big\}\,\mathrm{d}\Omega = 0, \\
&\int\!\!\int_\Omega \{j\omega\rho_0\tau w_\tau + (\gamma-1)T_0\rho_0 w_\tau(\partial_r v_r + \partial_z v_z + v_r/r) \\
&\quad + \gamma\lambda_h(\partial_r\tau\partial_r w_\tau + \partial_z\tau\partial_z w_\tau)/C_P\}\,\mathrm{d}\Omega = 0,
\end{aligned} \tag{22}$$

where $\mathrm{d}\Omega = 2\pi r\,\mathrm{d}r\,\mathrm{d}z$, η is the bulk dynamic viscosity, w_{vr}, w_{vz}, and w_τ are the test functions related to the radial and axial components of the particle velocity v_r and v_z and to the temperature variation τ, respectively. Note that only the integrals on the fluid domain Ω appear in Eq. (22); the integrals on the boundary Γ of the fluid domain vanish either due to the homogeneous Neumann boundary condition or to vanishing test function for homogeneous Dirichlet boundary condition.

The acoustic pressure in the domain can be expressed in terms of variables $\boldsymbol{v},\tau$ using the fundamental conservation and state equations[12]

$$p(r,\, z) = \hat{\beta}\tau - \frac{\rho_0 c_0^2}{j\omega\gamma}\operatorname{div}\boldsymbol{v}. \tag{23}$$

The pressure at the membrane $p(r,\, z=0)$ accounts for the source term of the equation governing the membrane displacement (1) whose weak form is expressed as follows:

$$\int_{\Gamma_M}\{-\partial_r\xi\partial_r w_\xi + K^2\xi w_\xi + w_\xi(p(r,z=0)-p_{inc})/T\}\,\mathrm{d}\Gamma_M = 0, \tag{24}$$

where Γ_M is the membrane part of the domain boundary, $\mathrm{d}\Gamma_M = 2\pi r\,\mathrm{d}r$, and w_ξ is the test functions related to the membrane displacement, ξ. This coupling between Eqs. (22) and (24) is completed by the boundary condition for the axial component of the particle velocity, $v_z = j\omega\xi$ on Γ_M. The membrane is assumed to be isothermal ($\tau = 0$ on Γ_M). Concerning the other parts of the domain boundary, the usual non-slip and isothermal boundary conditions ($\boldsymbol{v} = \boldsymbol{0}, \tau = 0$) on the rigid isothermal boundaries and the conditions of symmetry ($\partial_r v_z = 0$, $v_r = 0$, and $\partial_r\tau = 0$) on the z-axis are accounted for.[10,11]

IV. RESULTS AND DISCUSSION

Several examples of analytical (using first ten eigenmodes) and numerical results on the membrane displacement field, the acoustic pressure field behind the membrane, and receiver pressure sensitivity, as a function of the frequency, are presented hereafter. The physical parameters that specify the properties of the fluid (air, in this case) are given in Table I (the value of the bulk dynamic viscosity, η, is calculated from the value of the shear dynamic viscosity, μ, using equation[14] $\eta = 0.6\mu$).

The comparison between the analytical and numerical results for the membrane displacement field $\xi(r)$ and the acoustic pressure behind the membrane $p(r, z=0)$ at 1 kHz, 50 kHz, and 100 kHz is shown in Fig. 2. The incident pressure is set to 1 Pa; the dimensions and other parameters of the transducer which correspond to MEMS microphone[4,5,15,16] are given in Table II. The volume, V_c, and the

TABLE I. Parameters of the thermoviscous fluid.

Parameter	Value	Unit
Static pressure, P_0	101 325	Pa
Static temperature, T_0	296.15	K
Density, ρ_0	1.180	$\mathrm{kg\,m^{-3}}$
Adiabatic speed of sound, c_0	345.9	$\mathrm{m\,s^{-1}}$
Shear dynamic viscosity, μ	1.830×10^{-5}	Pa s
Bulk dynamic viscosity, η	1.098×10^{-5}	Pa s
Thermal conductivity, λ_h	24.40×10^{-3}	$\mathrm{W\,m^{-1}\,K^{-1}}$
Ratio of specific heats, γ	1.400	—
Specific heat coefficient at constant pressure per unit of mass, C_P	1.010×10^{3}	$\mathrm{J\,kg^{-1}\,K^{-1}}$

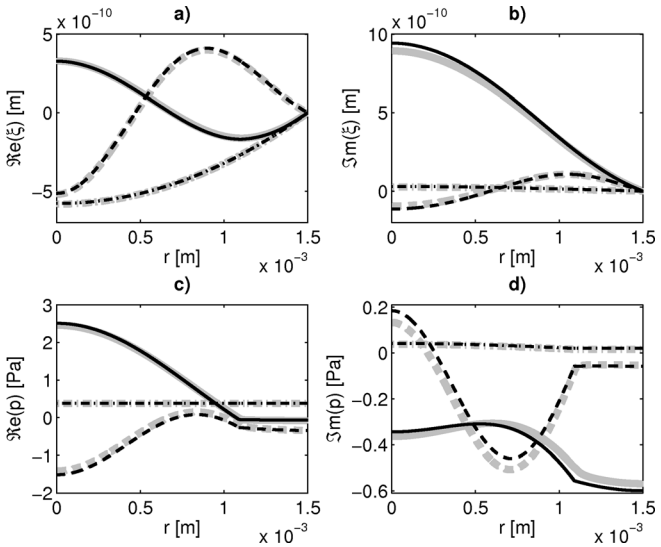

FIG. 2. Comparison of the analytical (black lines) and numerical (gray lines) results for the (a) real and (b) imaginary parts of the membrane displacement, and the (c) real and (d) imaginary parts of the acoustic pressure behind the membrane at 1 kHz (dashed-dotted lines), 50 kHz (solid lines), and 100 kHz (dashed lines).

thickness, h_c, of the cavity determine the radius of the electrode, $R_e = 1.09$ mm. A good agreement between the analytical and numerical results is obtained. A discontinuity of the first derivative with respect to radial coordinate of the acoustic pressure behind the membrane can be observed in the analytical results. This is due to the approximate continuity condition which involves the volume velocity at $r = R_e$ (the continuity of the z-dependent radial particle velocity would be more appropriate), but the comparison with the numerical results shows that this approximation remains acceptable. The mappings of the numerically calculated acoustic pressure, $p(r, z)$, in the cavity at 1 kHz, 50 kHz, and 100 kHz depicted in Fig. 3 show that the approximation used in the analytical solution assuming only r-dependent acoustic pressure (see Sec. II B 1) is valid in the major part of the cavity. The imperfect validity of this approximation in the small

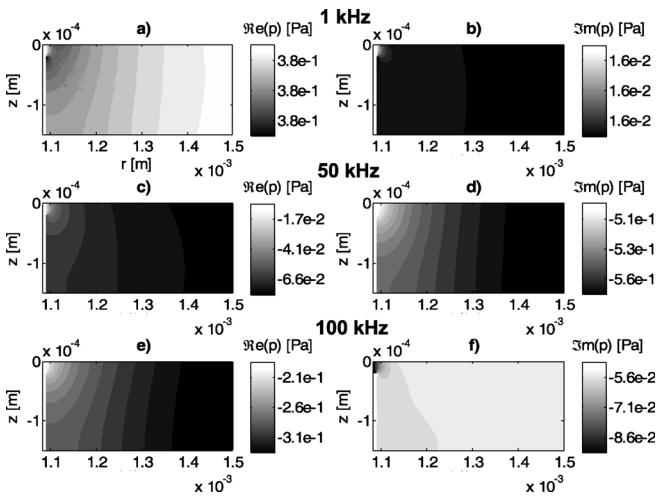

FIG. 3. Acoustic pressure in the cavity calculated numerically: at 1 kHz, (a) real and (b) imaginary parts; at 50 kHz, (c) real and (d) imaginary parts; and at 100 kHz, (e) real and (f) imaginary parts.

TABLE II. Dimensions and other parameters of the transducer.

Parameter	Value	Unit
Air gap thickness, h_g	20×10^{-6}	m
Cavity volume, V_c	5×10^{-10}	m^3
Cavity thickness, h_c	150×10^{-6}	m
Membrane radius, R_M	1.5×10^{-3}	m
Membrane thickness, h_M	10×10^{-6}	m
Silicon membrane density, ρ_M	2330	$kg\,m^{-3}$
Membrane tension, T	600	$N\,m^{-1}$
Polarization voltage, U_0	30	V

region near the geometrical discontinuity has negligible impact on the calculated membrane displacement (the variable of interest when calculating the pressure sensitivity of the transducer), as shown in Fig. 2.

The transducer considered herein is compared in terms of sensitivity and bandwidth with the previously described transducer with planar backing electrode of the same radius as the one of the membrane, the peripheral cavity being set outside the periphery of the membrane[1] as shown in Fig. 4, both having exactly the same properties (given in Table II), the external dimension of the second one, $R_c = 1.8196\,mm$ (equal to the dimension of the external periphery of the outer cavity), being determined by the volume, V_c, and the thickness, h_c, of the peripheral cavity. The pressure sensitivities of these two transducers as functions of the frequency, both being calculated analytically and numerically, are presented in Fig. 5. First, good agreement between the analytical and numerical results can be noticed. Second, the comparison shows that the transducer considered herein is advantageous in terms of pressure sensitivity and bandwidth; its sensitivity at 100 Hz is 0.654 mV/Pa (−63.68 dB re 1 V/Pa) against 0.478 mV/Pa (−66.41 dB re 1 V/Pa) for the previously described transducer, even though both have the same geometrical and mechanical properties. Moreover, in the transducer considered herein, the first eigenmode is less damped, which means that its dimensions (particularly, the air gap thickness, h_g, and the electrode radius, R_e) can be optimized, and its sensitivity and bandwidth can be further improved. Note that the sensitivity curves appear coherent with the mean value of the displacement field over the surface of the electrode, S_e.

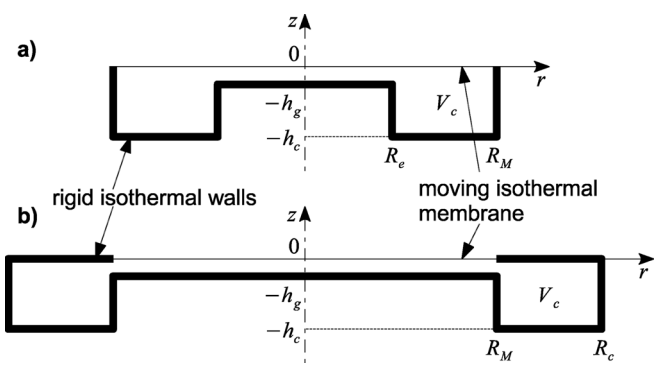

FIG. 4. Comparison of geometries of (a) the transducer described herein and (b) the previously described transducer (Ref. 1; the same properties for both transducers are given in Table II).

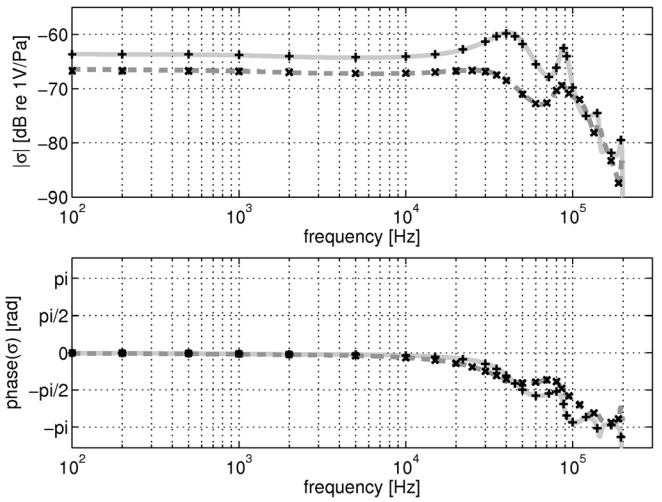

FIG. 5. Magnitude (upper curves) and phase (lower curves) of pressure sensitivity of the transducers: comparison of the analytical (lighter gray solid line) and numerical ("+" marks) results for the transducer considered herein and analytical (darker gray dashed line) and numerical ("×" marks) results for the previously described transducer (Ref. 1; the same properties for both transducers are given in Table II).

The analytical pressure sensitivities of the optimized transducers presented herein are compared with the one from the previously described transducer in Fig. 6. Apart from the improved sensitivity and bandwidth, another remarkable property can be observed: the optimized transducers act as low-pass filters with a good selectivity which can be of interest from the point of view of the signal processing at the receiver's output. When the strongly decreasing part of the sensitivity curve, which occurs in the upper frequency domain (above 80 kHz), reaches the lowest value of the oscillations which appears in the pass-band of the transducer, we assume that the corresponding value of the frequency could

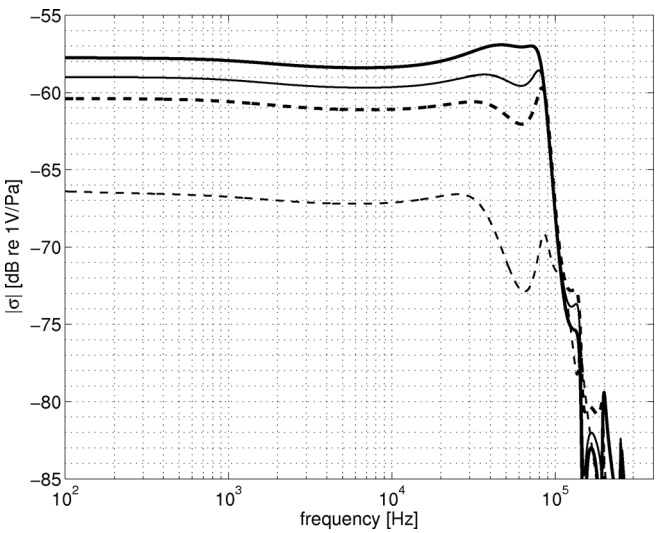

FIG. 6. Magnitudes of analytical pressure sensitivities of optimized receivers: configuration number 1 with $h_g = 15\ \mu m$ and $R_e = 1\,mm$ (thick dashed line), configuration number 2 with $h_g = 14\ \mu m$ and $R_e = 0.9\,mm$ (thin solid line), and configuration number 3 with $h_g = 13\ \mu m$ and $R_e = 0.81\,mm$ (thick solid line) compared to pressure sensitivity of the previously described transducer (Ref. 1) with dimensions given in Table II (thin dashed line).

TABLE III. Analytically calculated pressure sensitivities, upper frequency limits, and pass-band ripples of the receivers with optimized dimensions.

Configuration Number	h_g [μm]	R_e [mm]	σ_{LF} [mV/Pa]/[dB re 1 V/Pa]	f_{max} [kHz]	Ripple [dB]
1	15	1	0.956/−60.39	90.966	2.36
2	14	0.9	1.122/−59.00	85.480	1.09
3	13	0.81	1.292/−57.77	82.349	1.49

arbitrarily, but logically, represent the upper limit of the frequency bandwidth, f_{max} (then defined in this way). The pass-band ripple is then defined as the difference between the maxima and minima of the oscillations in dB. The optimized dimensions of these transducers, their sensitivities at 100 Hz σ_{LF}, the upper limits of the frequency bandwidth f_{max}, and the pass-band ripples are given in Table III. The first optimized transducer configuration has the highest upper frequency limit, the second one has the lowest pass-band ripple, and the third one has the highest sensitivity. It is worth noting that the two first eigenfrequencies, f_m ($m = 1, 2$), of the membrane *in vacuo* given by the solution of equation $J_0((2\pi f_m/\sqrt{T/m_s})R_M) = 0$ are equal, respectively, to $f_1 = 40.9$ kHz and $f_2 = 94.0$ kHz. Then, it appears that the sensitivity of the microphone presented herein drops off beyond the second mode of the membrane (when the dimensions are optimized in order to achieve appropriate damping), not beyond the first one as is the case for classical microphones.

V. CONCLUSION

In the device considered herein, the radius of the backing electrode is smaller than the radius of the membrane in order to allow to set a peripheral cavity around it, behind the peripheral part of the membrane, thus improving the compactness of the device while bringing a geometrical simplicity that is advantageous from a point of view of microfabrication. Despite the fact that the radius of the electrode is reduced in this way, this device can lead to both a higher sensitivity and a larger frequency bandwidth compared with the ones achieving other designs. These results are obtained from using both analytical and numerical modeling, which are relevant to interpret the phenomena involved in this kind of device; these theoretical approaches being validated previously from comparison with experimental results obtained on a similar transducer, and are available in the literature.

[1]M. Bruneau, A.-M. Bruneau, Z. Škvor, and P. Lotton, "An equivalent network modelling the strong coupling between a vibrating membrane and a fluid film," Acta Acust. Acust. **2**, 223–232 (1994).
[2]J. Škvor and Z. Škvor, "Electrostatic transducer with a nonplanar back plate," Eurosensors XVI Book of Abstracts **1–3**, 353–354 (2002).
[3]P. Honzík, Z. Škvor, S. Durand, and M. Bruneau, "Electrostatic transducer with square membrane and non-planar back plate: Simplified model," Acta Acust. Acust. **95**(5), 671–686 (2009).
[4]T. Le Van Suu, S. Durand, and M. Bruneau, "Fluid layer trapped between a plane, circular membrane and an axisymmetrically curved, smooth backing wall: Analytical model of the dynamic behaviour," Acta Acust. Acust. **94**(3), 474–482 (2008).
[5]T. Le Van Suu, S. Durand, and M. Bruneau, "On the modelling of clamped plates loaded by a squeeze fluid film: Application to miniaturised sensors," Acta Acust. Acust. **96**(5), 923–935 (2010).
[6]A. J. Zuckerwar, "Theoretical response of condenser microphones," J. Acoust. Soc. Am. **64**(5), 1278–1285 (1978).
[7]T. Lavergne, S. Durand, M. Bruneau, and N. Joly, "Dynamic behavior of the circular membrane of an electrostatic microphone: Effect of holes in the backing electrode," J. Acoust. Soc. Am. **128**(6), 3459–3477 (2010).
[8]D. Homentcovschi and R. N. Miles, "An analytical-numerical method for determining the mechanical response of a condenser microphone," J. Acoust. Soc. Am. **130**(6), 3698–3705 (2011).
[9]N. Joly, M. Bruneau, and R. Bossart, "Coupled equations for particle velocity and temperature variation as the fundamental formulation of linear acoustics in thermo-viscous fluids at rest," Acta Acust. Acust. **92**(2), 202–209 (2006).
[10]N. Joly, "Finite element modeling of thermoviscous acoustics on adapted anisotropic meshes: Implementation of the particle velocity and temperature variation," Acta Acust. Acust. **96**(1), 102–114 (2010).
[11]P. Honzík, N. Joly, S. Durand, D. Rodrigues, J.-N. Durocher, and M. Bruneau, "Finite element modelling of acoustic field inside small components: Application to an annular slit terminated by an aperture in an infinite screen," Metrologia **49**, 32–40 (2012).
[12]M. Bruneau and T. Scelo, *Fundamentals of Acoustics* (ISTE, London, 2006).
[13]D. Rodrigues, C. Guianvarc'h, J.-N. Durocher, M. Bruneau, and A.-M. Bruneau, "A method to measure and interpret input impedance of small acoustic components," J. Sound Vib. **315**(4–5), 890–910 (2008).
[14]A. D. Pierce, *Acoustics: An Introduction to Its Physical Principles and Applications* (McGraw-Hill, New York, 1981), p. 553, Eq. 10-7.23.
[15]P. Scheeper, A. V. D. Donk, W. Olthuis, and P. Bergveld, "A review of silicon microphones," Sens. Actuators, A **44**, 1–11 (1994).
[16]C. W. Tan and J. M. Miao, "Analytical modeling for bulk-micromachined condenser microphones," J. Acoust. Soc. Am. **120**(2), 750–761 (2006).